

Rethinking Open-Vocabulary Segmentation of Radiance Fields in 3D Space

Hyunjee Lee*, Youngsik Yun*, Jeongmin Bae, Seoha Kim, Youngjung Uh†

Yonsei University
 {hyunji12, bbangsik, jaymin.bae, hailey07, yj.uh}@yonsei.ac.kr

Abstract

Understanding the 3D semantics of a scene is a fundamental problem for various scenarios such as embodied agents. While NeRFs and 3DGS excel at novel-view synthesis, previous methods for understanding their semantics have been limited to incomplete 3D understanding: their segmentation results are rendered as 2D masks that do not represent the entire 3D space. To address this limitation, we redefine the problem to segment the 3D volume and propose the following methods for better 3D understanding. We directly supervise the 3D points to train the language embedding field, unlike previous methods that anchor supervision at 2D pixels. We transfer the learned language field to 3DGS, achieving the first real-time rendering speed without sacrificing training time or accuracy. Lastly, we introduce a 3D querying and evaluation protocol for assessing the reconstructed geometry and semantics together. Code, checkpoints, and annotations are available at the project page.

Project page — <https://hyunji12.github.io/Open3DRF/>

1 Introduction

Semantically understanding 3D space is important for various computer vision tasks. For instance, it is crucial to segment 3D objects accurately for robot manipulation (Rashid et al. 2023; Zheng et al. 2024). Recently, several works have focused on understanding 3D scenes represented by radiance fields such as Neural Radiance Fields (NeRFs) (Mildenhall et al. 2020) and 3D Gaussian Splatting (3DGS) (Kerbl et al. 2023). LERF (Kerr et al. 2023) introduces a language embedding field which is rendered on a chosen viewpoint to be queried by open vocabulary. The language field is supervised by CLIP (Radford et al. 2021) embeddings from the multi-scale patches to capture various sizes of objects. Subsequent works (Zhang, Li, and Ahuja 2024; Qin et al. 2023) incorporate SAM masks (Kirillov et al. 2023) to supervise the language field for clear segmentation boundaries.

We revisit the 3D understanding of NeRFs and 3DGS in four aspects: problem setting, supervision, embeddings, and evaluation. The problem setting of previous works leads to limited 3D understanding as they merely produce rendered

*These authors contributed equally.

†Corresponding author.

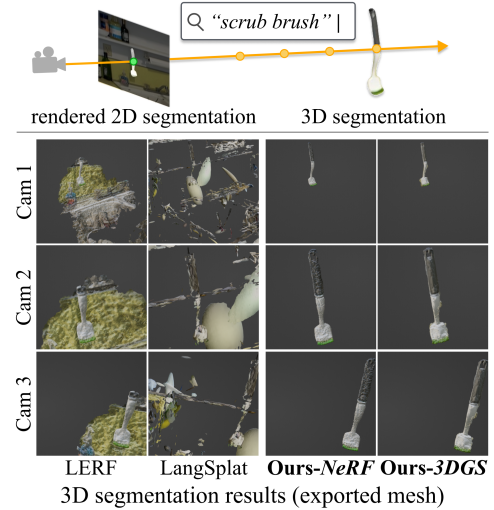


Figure 1: Previous works segment rendered 2D masks on rendered features to understand radiance fields. Instead, we reformulate the task to segment 3D volumes. Our approach significantly improves 3D understanding of radiance fields.

2D masks for given viewpoints rather than 3D semantic volumes. On the other hand, we set the problem to segment 3D volume regarding the semantics of 3D points.

The previous methods encourage the rendered embeddings, rather than the embeddings in 3D space, to match the ground truth. Furthermore, their multi-scale language embeddings require finding the optimal scale for a given viewpoint and a query text, which is prone to multi-view inconsistency. In contrast, we encourage 3D points to learn language embeddings following our revisited problem setting. Although the ground truth is still language embeddings of 2D images, changing the dimension for computing the loss greatly improves 3D understanding as shown in Figure 1. In addition, we remove multi-scale embeddings by encoding masked objects, achieving multi-view consistent rendered feature maps.

Meanwhile, previous works on understanding 3DGS explicitly add language embeddings for each Gaussian and jointly train them (Qin et al. 2023; Zhou et al. 2023). However, directly appending a 512-dimensional language em-

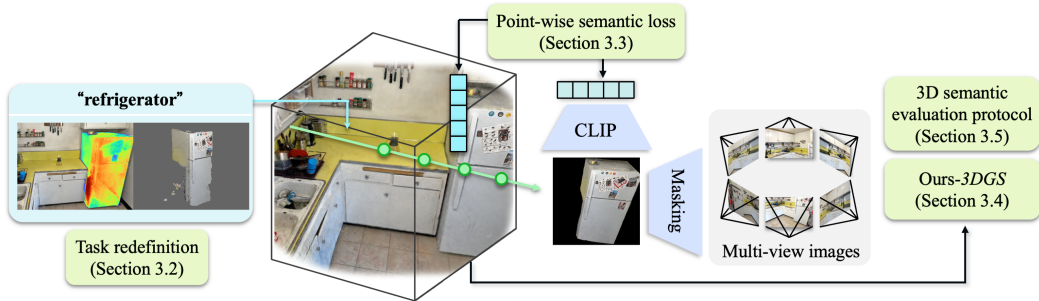


Figure 2: We propose 3D segmentation as a more practical problem setting, segmenting the 3D volume for a given text query (Section 3.2). Then we propose point-wise semantic loss to supervise the sampled point embeddings (Section 3.3). Furthermore, the learned language fields can be transferred into 3DGS for faster rendering speeds (Section 3.4). Lastly, our 3D evaluation protocol measures the 3D segmentation performance both in reconstructed geometry and semantics (Section 3.5).

bedding to each Gaussian and rendering them result in out-of-memory (OOM) issues. Hence, they either 1) compress language embeddings to low-dimensional features, significantly sacrificing the accuracy (Shi et al. 2023; Qin et al. 2023), or 2) modify the rasterizer, which is slow for training (Zhou et al. 2023; Ye and Kanazawa 2023). To overcome these drawbacks, we transfer our learned language field into 3DGS to enable the real-time rendering of the accurate language field.

Our final aspect is evaluation. Existing works measure mIoU *in pixels* between the rendered 2D masks and the 2D ground truth, or measure mIoU *on ground truth point clouds* ignoring the reconstructed geometry (Engelmann et al. 2024). However, 3D understanding should know the correct 3D volume of a target semantics. Therefore, the evaluation method should assess semantics and the reconstructed geometry together. Accordingly, we propose to evaluate the accuracy of 3D understanding as the agreement between estimated volume in mesh and ground truth mesh, measured in F1-score. The proposed evaluation is applicable to both NeRF and 3DGS.

In the experiments, we demonstrate the superiority of our method regarding 1) 3D and rendered 2D segmentation accuracy, 2) training and rendering time, and 3) consistency across viewpoints.

In summary, our contributions are:

- We propose a practical problem setting for 3D understanding of NeRFs and 3DGS.
- We propose to directly supervise 3D points before volume rendering to learn a language embedding field. It achieves the state-of-the-art accuracy in 3D and rendered 2D segmentation.
- We propose to transfer the language field to 3DGS. It achieves the first real-time rendering speed among open-vocabulary methods which is $28\times$ faster than the previous fastest method.
- We propose a 3D evaluation protocol between estimated volume and ground truth volume represented as meshes.

2 Related Work

In this section, we briefly review neural 3D scene representations, especially NeRF and 3DGS, and then discuss the semantic understanding of 3D scenes.

Radiance Fields NeRF (Mildenhall et al. 2020) reconstructs a scene as a continuous function that maps 3D points to radiance and density values. Volume rendering pipeline renders the points to determine the color of each pixel on an image from an arbitrary perspective. Rather than volumetric rendering, 3DGS (Kerbl et al. 2023) achieves fast rendering speeds by projecting 3D Gaussians onto the camera plane followed by depth-sorted alpha-blending. Each 3D Gaussian stores location, rotation, scale, opacity, and color. Recent studies use these representations to semantically understand 3D scenes for various applications such as robotics (Rashid et al. 2023; Wang et al. 2023; Zheng et al. 2024; van Oort et al. 2024; Li and Pathak 2024).

Semantic Understanding of Radiance Field The most straightforward way to understand 3D scenes represented by neural radiance fields is by adding an auxiliary branch for semantic segmentation (Zhi et al. 2021; Bing, Chen, and Yang 2022; Liu et al. 2023; Ye et al. 2023). This approach allows synthesizing semantic masks from novel views but requires a pre-defined list of target classes before training, called *closed-set*. Therefore, retraining or using additional models for untrained queries is necessary, limiting application for open-vocabulary scenarios. As vision-language model (VLM) features (e.g., CLIP (Radford et al. 2021)) expand the semantic understanding to *open-set*, it becomes a widely used approach to distill CLIP features into 3D scenes.

LERF (Kerr et al. 2023) pre-computes multi-scale patches to prepare multi-scale ground-truth CLIP features. Similar to LERF, FMGS (Zuo et al. 2024) pre-computes multi-scale ground-truth CLIP features and averages them to generate a low-resolution hybrid feature map for training. Instead of using patches, LEGaussians (Shi et al. 2023) distills pixel-level CLIP features. Similarly, OpenNeRF (Engelmann et al. 2024) computes pixel-level CLIP features using OpenSeg (Ghiasi et al. 2022). GOI (Qu et al. 2024) trains the codebook to compress the high-dimensional se-

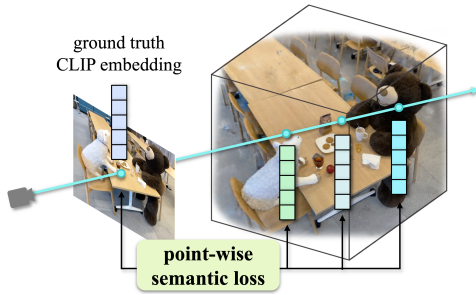


Figure 3: Point-wise semantic loss supervises the language embeddings of sampled points directly in 3D space, ensuring precise semantics.

mantic features into low-dimensional vectors¹. As it produces mixed CLIP features to contain multiple objects into a patch, LangSplat (Qin et al. 2023) utilizes SAM (Kirillov et al. 2023) to create patches for a single object. OpenMask3D (Takmaz et al. 2023) creates a bounding box from the SAM mask, and crops the image to make per-mask features. However, OpenMask3D uses bounding box, which still leads to mixed CLIP features. Since studies using multi-scale feature maps select the most relevant scale, different scales can be chosen at different views with the same query, leading to multi-view inconsistent results (Kerr et al. 2023; Qin et al. 2023; Shi et al. 2023). On the other hand, we use SAM to make the field free from scales.

Language Embedded 3DGS Directly embedding high-dimensional CLIP features into each Gaussian is infeasible due to the limited GPU shared memory. Therefore, recent studies for understanding open-vocabulary 3D segmentation using 3D as a backbone address this problem in two ways. LEGaussians and LangSplat compress the CLIP features using an autoencoder (Shi et al. 2023; Qin et al. 2023). However, they need to optimize the autoencoder for each scene and endure performance degradation. Others using 3DGS without feature compression (Zhou et al. 2023; Labe et al. 2024) utilize global memory, suffering for longer training time. Meanwhile, we effectively optimize 3DGS transferred from our learned language field, without the above trade-off.

3 Methods

First, we provide preliminary on LERF (Kerr et al. 2023). Then we redefine 3D segmentation of radiance fields as computing 3D relevancy scores. Accordingly, we introduce point-wise semantic loss to supervise ray points in 3D space by our scale-free embeddings. In addition, we propose to transfer our learned language field into 3DGS for real-time rendering. Lastly, we introduce the evaluation protocol for 3D segmentation. Figure 2 illustrates an overview.

¹At the time of this work, the code of GOI was unavailable. However, its released code showed 15 fps on LERF dataset, falling short of real-time rendering.

3.1 Preliminary: LERF

For open-vocabulary segmentation, LERF builds an additional language field on top of iNGP (Müller et al. 2022). The language field F_{lang} is jointly trained with the radiance field by querying point embeddings $F_{\text{lang}}(\mathbf{x}, s)$ at N sample points' position \mathbf{x} and scale s along each ray. The 3D point language embeddings are then accumulated via the volume rendering (Max 1995) to obtain rendered language embedding $\hat{\phi}_{\text{lang}}^s$ in 2D pixel space: $\hat{\phi}_{\text{lang}}^s = \sum_{i=0}^N w_i F_{\text{lang}}(\mathbf{x}_i, s)$. The weight of each sampled point is calculated as $w_i = T_i(1 - \exp(-\sigma_i \delta_i))$, where $T_i = \exp(-\sum_{j=1}^{i-1} \sigma_j \delta_j)$ is transmittance, δ is the distance between adjacent samples, and σ is the volume density. Then, the rendered embedding is normalized to the unit sphere as in CLIP: $\hat{\phi}_{\text{lang}}^s = \hat{\phi}_{\text{lang}}^s / \|\hat{\phi}_{\text{lang}}^s\|$. To train the language field, LERF crops the training dataset into multi-scale patches, creating ground truth language embedding $\phi_{\text{lang}}^{\text{gt}}$ and maximizing the cosine similarity between the rendered language embedding $\hat{\phi}_{\text{lang}}^s$:

$$L_{\text{lang}} = - \sum_s \lambda_{\text{lang}} \phi_{\text{lang}}^s \cdot \phi_{\text{lang}}^{\text{gt}}. \quad (1)$$

Furthermore, LERF builds an additional branch for the DINO (Caron et al. 2021) feature field as an extra regularizer for achieving clearer object boundaries. Similar to the above, the DINO branch is trained to maximize the similarity between rendered DINO embedding $\hat{\phi}_{\text{dino}}^s$ and the DINO ground truth $\phi_{\text{dino}}^{\text{gt}}$. The DINO branch is not used during inference.

For rendered 2D segmentation, LERF computes the relevancy score using the rendered embeddings $\hat{\phi}_{\text{lang}}^s$ and obtains the 2D mask:

$$\min_i \frac{\exp(\hat{\phi}_{\text{lang}}^s \cdot \phi_{\text{text}})}{\exp(\hat{\phi}_{\text{lang}}^s \cdot \phi_{\text{text}}) + \exp(\hat{\phi}_{\text{lang}}^s \cdot \phi_{\text{canon}}^i)}. \quad (2)$$

3.2 Task Redefinition

Existing methods provide limited 3D semantic understanding for given texts via *rendered* 2D masks on viewpoints that do not directly represent the entire 3D space. Instead, we propose *3D segmentation* as a more practical problem setting: segmenting the 3D volume for given texts. While following the basic elements of language embeddings and relevancy scores, we compute relevancy scores of the language embeddings queried *on 3D points* \mathbf{x} instead of the ones rendered on 2D images:

$$\min_i \frac{\exp(F_{\text{lang}}(\mathbf{x}) \cdot \phi_{\text{text}})}{\exp(F_{\text{lang}}(\mathbf{x}) \cdot \phi_{\text{text}}) + \exp(F_{\text{lang}}(\mathbf{x}) \cdot \phi_{\text{canon}}^i)}, \quad (3)$$

where ϕ_{canon}^i represents predefined canonical texts such as *photo* and *image*. In NeRFs, we compute the relevancy scores on the points along the rays through pixels. For 3DGS, we compute the relevancy scores on the center positions of the Gaussians. The regions where the computed relevancy scores surpass the selected threshold are considered object regions.

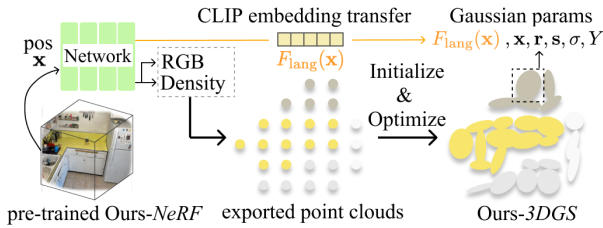


Figure 4: Transferring Ours-NeRF into 3DGS: We initialize 3DGS using the point cloud exported from our learned NeRF, then optimize the attributes of 3DGS except for position. The language features obtained by querying the language field at the Gaussian center positions are then transfer to 3DGS.

3.3 Supervising Semantics in 3D Space

It is a reasonable choice to minimize the error between the rendered colors and the ground truth colors on 2D images for novel view synthesis. In contrast, the similar objective for language embeddings (Eq. (1)) harms correctly understanding 3D semantics as shown in Figure 1.

To address this issue, we propose a point-wise semantic loss which uses CLIP embeddings $\phi_{\text{lang}}^{\text{gt}}$ as direct ground truth for the embeddings of 3D points on the ray $F_{\text{lang}}(\mathbf{x})$. Specifically, we maximize the similarity between point embeddings $F_{\text{lang}}(\mathbf{x})$ and the ground truth CLIP embedding $\phi_{\text{lang}}^{\text{gt}}$:

$$L_{\text{PS}} = - \sum_{i=0}^N (w_i F_{\text{lang}}(\mathbf{x}_i) \cdot \phi_{\text{lang}}^{\text{gt}}). \quad (4)$$

We also apply the same approach described above for DINO regularization. We show that point-wise semantic loss improves not only 3D segmentation but also rendered 2D segmentation thanks to a better understanding of 3D semantics.

Notably, multi-scale approaches (Kerr et al. 2023; Qin et al. 2023) lead to multi-view inconsistency because these approaches have language embedding per scale and different views may have different optimal scales. To address this, we use SAM (Kirillov et al. 2023) to obtain object masks and create scale-free ground truth CLIP embeddings by masking out their background and cropping tightly to the masks. It ensures view-consistent language fields without the need to determine the optimal scale. We note that previous methods with SAM still model multi-scale CLIP embedding fields (Zhang, Li, and Ahuja 2024; Qin et al. 2023).

3.4 Transferring Language Field into 3DGS

A straightforward approach for the same task with 3DGS is to jointly optimize the Gaussians and their additional language embeddings, which requires vast memory consumption. It suffers from slow training² (Zhou et al. 2023), or requires an additional model for feature compression, which

²Training on GPU global memory is slow due to the gradient computation in the backward pass. The forward pass is still fast.

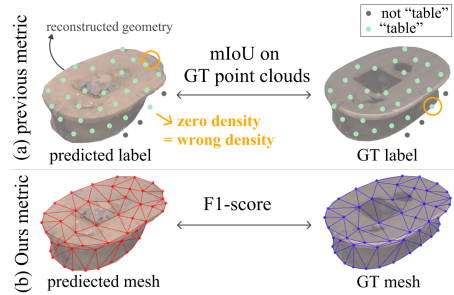


Figure 5: Comparison of 3D Evaluation: (a) Existing methods predict the labels at the ground truth point cloud. It is misleading when the language embeddings capture the object area while the reconstructed geometry does not cover that object area. (b) To address this problem, we extract 3D meshes from the segmented points of the reconstructed scene to measure the F1-score between the exported mesh and the ground truth mesh.

degrades accuracy due to compression loss (Shi et al. 2023; Qin et al. 2023). Appendix provides more details.

To tackle this problem, we propose to simply bake our learned language field into 3DGS by querying the language embedding at the center of the Gaussians. The queried embeddings are frozen. It runs instantly (22ms) and still allows fast rendering².

In addition, we propose to initialize the center coordinates of 3DGS from the learned radiance field. We collect ray points and extract the top 1M points regarding density following NeRFstudio (Tancik et al. 2023). Unlike previous methods (Niemeyer et al. 2024), we implement this approach to align the geometry of 3DGS with the language field. Therefore, we freeze the center position of the Gaussians \mathbf{x} , without densification or pruning during training. We then transfer language embeddings $F_{\text{lang}}(\mathbf{x})$ at the center of Gaussians.

Similar to previous methods, we modify the rasterizer to render high-dimensional language features (see Appendix). The rendered language embedding $\hat{\phi}_{\text{lang}}$ is obtained by α -blending:

$$\hat{\phi}_{\text{lang}} = \sum_{i \in N} F_{\text{lang}}(\mathbf{x}_i) \alpha_i \prod_{j=1}^{i-1} (1 - \alpha_j), \quad (5)$$

where N denotes the number of Gaussians overlapping on the pixel. The alpha value is calculated as $\alpha_i = \sigma_i G(\mathbf{x}_i)$, where G denotes the Gaussian kernel and σ denotes the opacity of Gaussians. We use Eq. (3) for 3D segmentation.

3.5 3D Semantic Evaluation Protocol

A previous work (Engelmann et al. 2024) measures the mIoU between the prediction and annotation on the ground truth point cloud. It might incorrectly classify the points with zero density and a correct embedding, shown in Figure 5-(a).

To address this problem, we propose to measure the F1-score between the exported mesh from the segmented results

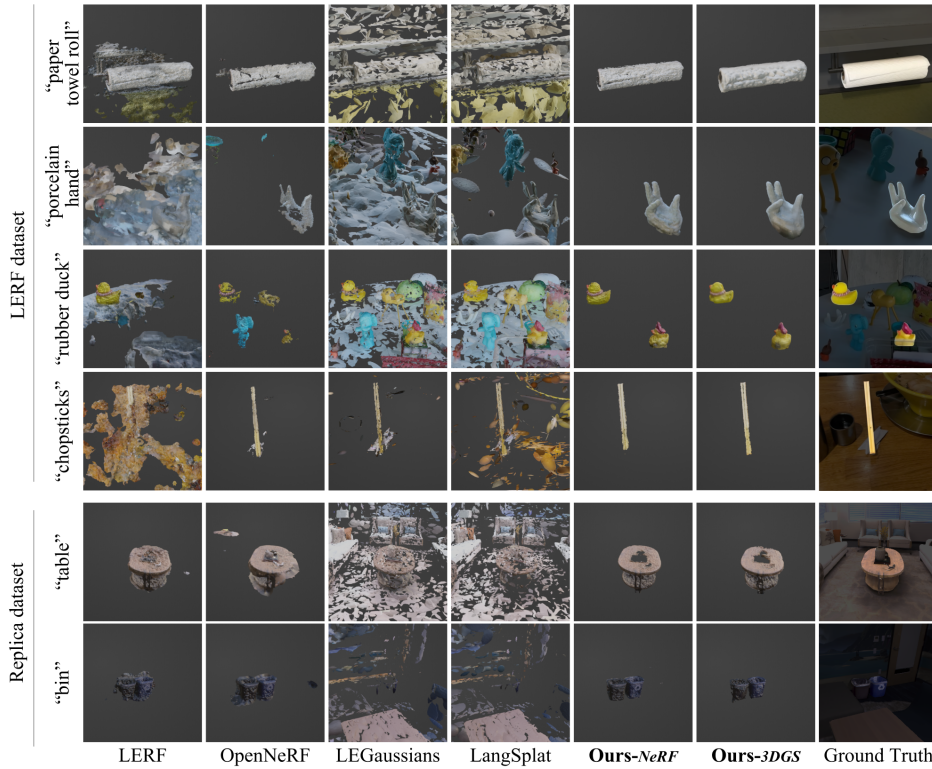


Figure 6: Qualitative comparisons of 3D segmentation on LERF and Replica datasets: We show an exported mesh of 3D querying results for the given text query. Unlike competitors, our method produces more clear boundaries in 3D segmentation results.

to ground truth mesh, inspired by surface reconstruction literature (Knapitsch et al. 2017; Li et al. 2023). Precision computes the ratio of correct volume among the estimated volume. Recall computes the ratio of covered volume among the GT volume. As it is impractical to compute the volume, we approximate the volume by a regular grid points in the estimated and GT meshes. A point is considered *correct* or *covered* if there exists a point within a radius in the counterpart. We note that this protocol can be generally applied to various neural representations, such as NeRF or 3DGS.

4 Experiments

In this section, we evaluate our methods on various datasets and compare them to competitors in terms of 3D and rendered 2D segmentation with given text queries. We choose LERF, OpenNeRF, LEGaussians, and LangSplat as competitors, which are open-sourced. We re-evaluate the competitors using the official code³. Appendix provides details of the datasets.

Evaluation For quantitative comparison in 3D segmentation, we export meshes using the Poisson surface reconstruction. In LERF, OpenNeRF, and Ours-*NeRF*, we use Nerfs-

³The official implementation of LangSplat includes evaluation views during training, while we exclude them for fairness, following LERF and OpenNeRF.

Backbone	Method	Replica F1-score \uparrow
NeRF	LERF	0.0845
	OpenNeRF	0.0361
	Ours-<i>NeRF</i>	0.1520
3DGS	LEGAussians	0.0067
	LangSplat	0.0087
	Ours-<i>3DGS</i>	<u>0.1353</u>

Table 1: 3D Segmentation Accuracy Comparison on the Replica dataset. **Bold** indicates the 1st, and underline indicates the 2nd-best model.

studio (Tancik et al. 2023) to export meshes with 30K sampled points. In LEGaussians, LangSplat and Ours-*3DGS*, we use SuGaR (Guédon and Lepetit 2023) to export meshes. For rendered 2D segmentation, we evaluate the mIoU and mAP between the ground truth mask and the predicted mask. For qualitative comparison in 3D segmentation, we use 50K points for Nerfstudio in LERF, OpenNeRF, and Ours-*NeRF*.

4.1 Segmentation Accuracy

3D Segmentation We compare qualitative results of 3D segmentation by exporting meshes for the region obtained

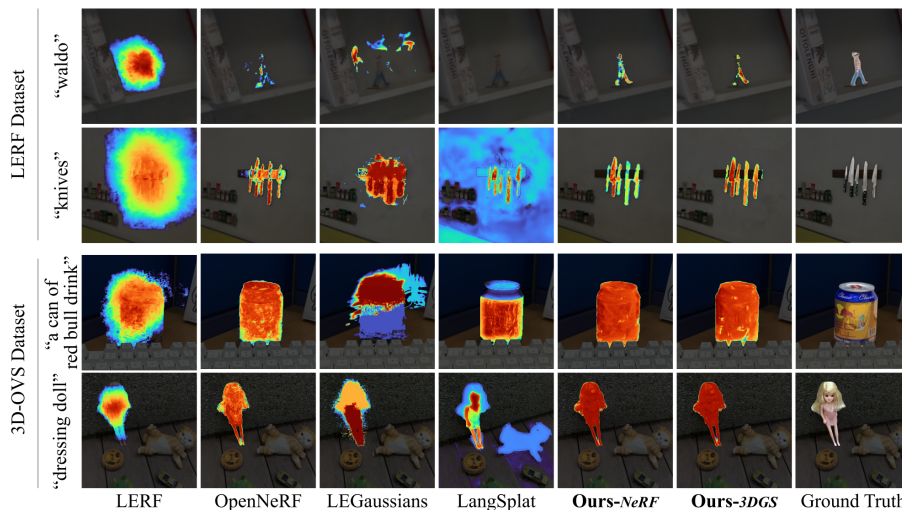


Figure 7: Comparisons of Rendered 2D Segmentation on LERF and 3D-OVS datasets: We show a heatmap of the similarity for the given text query. We dim the background except for the target object, for better visualization. Our method achieves accurate segmentation results compared to competitors.

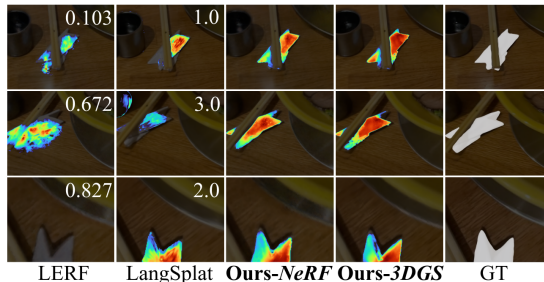


Figure 8: Comparison of view consistency: The figure shows the optimal scales of LERF and LangSplat for each viewpoint on `napkin` in LERF dataset, highlighting significant variation and view inconsistency in competitors. Our method avoids this by utilizing scale-free embeddings.

through 3D querying (Section 3.2). In Table 1, both of our models surpass the competitors.

In Figure 6, unlike competitors, *Ours-NeRF* and *Ours-3DGS* produce clear segmentation boundaries of the target object from the 3D scene. Notably, both of our models accurately segment complex shape objects and multiple objects like `porcelain hand` and `rubber ducks`. In the `rubber duck` query, LERF, LEGaussians, and LangSplat completely fail to localize the target object, while OpenNeRF incorrectly segments unrelated objects (e.g., a toy elephant and Jake) along with the target object.

Rendered 2D Segmentation In Table 2, both of our models show the highest rendered 2D segmentation performance on LERF and 3D-OVS datasets. Also, we present qualitative results of rendered 2D segmentation by comparing a heatmap for given text queries through 2D querying (Section 3.2). As shown in Figure 7, *Ours-NeRF* and *Ours-3DGS* show clear segmentation boundaries. LangSplat and

Method	LERF		3D-OVS	
	mIoU \uparrow	mAP \uparrow	mIoU \uparrow	mAP \uparrow
LERF	31.88	30.44	52.60	57.03
OpenNeRF	26.52	25.84	75.12	75.35
Ours-NeRF	46.37	45.86	<u>77.46</u>	<u>84.65</u>
LEGaussians	21.43	20.81	47.98	50.86
LangSplat ³	37.53	36.39	74.54	79.49
Ours-3DGS	<u>44.37</u>	<u>44.57</u>	77.51	84.86

Table 2: Quantitative Results of Rendered 2D Segmentation on LERF and 3D-OVS datasets.

LEGaussians occasionally fail to find the target object, as seen with `waldo`.

Figure 8 shows relevancy maps and optimal scales along different viewpoints. The float value on the top right of the image represents the optimal scale for LERF and LangSplat from each viewpoint. In Figure 8, our method renders view consistent relevancy maps with `napkin` query. However, LERF and LangSplat show view inconsistent segmentation results due to the changing optimal scale.

4.2 Computational Time

Table 3 shows the computational times of the LERF `waldo_kitchen` scene with a single RTX A5000. We report the training time and rendering time for both ours and the competitors. LangSplat and LEGaussians train an autoencoder for each scene and require decoding during rendering. Note that LangSplat trains 3DGS from scratch, optimizes the language-embedded 3DGS per scale, heavily depends on post-processing (see Appendix). *Ours-3DGS* takes 40 minutes to train *Ours-NeRF*, 5 minutes to optimize 3DGS, and 22 milliseconds to query and transfer language field into

Backbone	Method	Training ↓	Rendering				
			Render ↓	Decode ↓	Post-Process ↓	FPS ↑	Real-Time
NeRF	LERF	40 mins	23688. ms	-	-	0.04	✗
	OpenNeRF	40 mins	5944.7 ms	-	-	0.17	✗
	Ours-NeRF	40 mins	2337.7 ms	-	-	0.43	✗
3DGS	LEGaussians	90 mins	15.665 ms	384.6 ms	-	<u>2.50</u>	✗
	LangSplat	100 mins	17.249 ms	0.935 ms	10473 ms	0.10	✗
	Ours-3DGS	40+5 mins	14.257 ms	-	-	70.1	✓

Table 3: Computational Time: We measure the computational cost on *waldo_kitchen* scene on an RTX A5000.

Method	Replica F1-score ↑	LERF		Computational Cost		
		mIoU ↑	mAP ↑	Training Time ↓	FPS ↑	# of Gaussians ↓
Ours-3DGS	0.1354	44.37	44.57	5 mins	70.1	1M
w/o NeRF init	0.1108	36.14	36.74	13 mins	41.2	2M

Table 4: Ablation Study of Initializing NeRF into 3DGS: The ablation is conducted on Replica dataset for 3D segmentation and on LERF dataset for rendered 2D segmentation. We measure the computational cost on *waldo_kitchen* scene with RTX A5000.

Method	Replica F1-score ↑	LERF	
		mIoU ↑	mAP ↑
Ours full	0.1532	46.37	45.86
w/o L_{PS}	0.0537	44.50	44.05
w/o $F_{lang}(\mathbf{x}_i)$	0.1114	30.03	28.85

Table 5: Ablation Study of Supervising Semantics in 3D Space: The datasets are Replica and LERF for 3D and rendered 2D segmentation, respectively. w/o L_{PS} denotes using LERF CLIP loss L_{lang} instead of point-wise semantic loss and w/o $F_{lang}(\mathbf{x}_i)$ denotes using multi-scale embedding $F_{lang}(\mathbf{x}_i, s)$ instead of scale-free embedding.

3DGS. Ours-3DGS achieves real-time rendering of language embeddings for the first time, $28\times$ faster than LEGaussians.

4.3 Ablation Study

Point-wise Semantic Loss We demonstrate the necessity of our point-wise semantic loss. Figure 9 qualitatively shows improvements due to point-wise semantic loss compared to 2D supervision with Eq. (1). Point-wise semantic loss removes meaningless floaters related to depth ambiguity. Table 5 shows that leveraging point-wise semantic loss instead of Eq. (1) makes better understanding in 3D space, improving the F1-score (+0.0995). Furthermore, point-wise semantic loss also indirectly improves rendered 2D segmentation accuracy.

Scale-Free Embedding Our scale-free language embedding field from SAM-segmented objects produce greatly improved accuracy with clear object boundaries compared to multi-scale embedding field. Figure 9 shows that scale-free embedding helps covering the head of the toy elephant which was lost with multi-scale embedding. In Table 5, the quantitative performance of the 3D and rendered 2D seg-

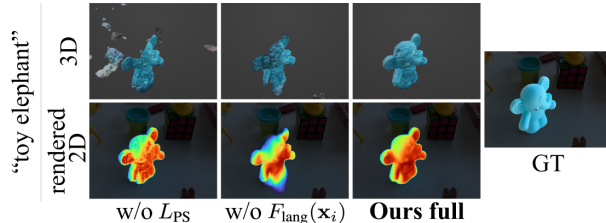


Figure 9: Qualitative Results of Ablation Study on *figurines* scene in LERF dataset.

mentation greatly improves using scale-free embedding.

NeRF Initialization We demonstrate the necessity of initializing 3DGS with the extracted point clouds from our learned NeRF. As shown in Table 4, training 3DGS with SfM (Schönberger and Frahm 2016) initialization with the densification and pruning leads to performance degradation in both 3D and rendered 2D segmentation. This indicates that aligning geometry and semantics is essential for transferring the language field to 3DGS. Moreover, NeRF initialization produces fewer Gaussians ($0.50\times$) which lead to less training time ($0.38\times$) and faster rendering speed ($1.70\times$).

5 Conclusion

We revisit the current literature on 3D understanding of NeRF and 3DGS and revise the problem setting. We reformulate the task to produce 3D segmented volumes instead of rendered 2D masks and propose a 3D evaluation protocol. We achieve state-of-the-art segmentation accuracy in both 3D and rendered 2D by computing loss directly on 3D points. Moreover, we enable the first real-time rendering speed among open-vocabulary methods by transferring the learned language field to 3DGS. We hope this paper drives forward a better 3D understanding of radiance fields by re-considering the problem set.

Acknowledgements

This work was supported by Institute of Information & communications Technology Planning & Evaluation(IITP) grant funded by the Korea government(MSIT) (No. RS-2024-00439762, Developing Techniques for Analyzing and Assessing Vulnerabilities, and Tools for Confidentiality Evaluation in Generative AI Models)

References

- Bhalgat, Y.; Laina, I.; Henriques, J. F.; Zisserman, A.; and Vedaldi, A. 2024. N2F2: Hierarchical Scene Understanding with Nested Neural Feature Fields. *arXiv:2403.10997*.
- Bing, W.; Chen, L.; and Yang, B. 2022. DM-NeRF: 3D Scene Geometry Decomposition and Manipulation from 2D Images. *arXiv preprint arXiv:2208.07227*.
- Caron, M.; Touvron, H.; Misra, I.; Jégou, H.; Mairal, J.; Bojanowski, P.; and Joulin, A. 2021. Emerging Properties in Self-Supervised Vision Transformers. *arXiv:2104.14294*.
- Dai, A.; Chang, A. X.; Savva, M.; Halber, M.; Funkhouser, T.; and Nießner, M. 2017. ScanNet: Richly-annotated 3D Reconstructions of Indoor Scenes. In *Proc. Computer Vision and Pattern Recognition (CVPR), IEEE*.
- Engelmann, F.; Manhardt, F.; Niemeyer, M.; Tateno, K.; and Tombari, F. 2024. OpenNerf: Open Set 3D Neural Scene Segmentation with Pixel-Wise Features and Rendered Novel Views. In *The Twelfth International Conference on Learning Representations*.
- Ghiasi, G.; Gu, X.; Cui, Y.; and Lin, T.-Y. 2022. Scaling Open-Vocabulary Image Segmentation with Image-Level Labels. *arXiv:2112.12143*.
- Guédon, A.; and Lepetit, V. 2023. SuGaR: Surface-Aligned Gaussian Splatting for Efficient 3D Mesh Reconstruction and High-Quality Mesh Rendering. *arXiv preprint arXiv:2311.12775*.
- Kerbl, B.; Kopanas, G.; Leimkühler, T.; and Drettakis, G. 2023. 3D Gaussian Splatting for Real-Time Radiance Field Rendering. *ACM Transactions on Graphics*, 42(4).
- Kerr, J.; Kim, C. M.; Goldberg, K.; Kanazawa, A.; and Tancik, M. 2023. LERF: Language Embedded Radiance Fields. In *International Conference on Computer Vision (ICCV)*.
- Kirillov, A.; Mintun, E.; Ravi, N.; Mao, H.; Rolland, C.; Gustafson, L.; Xiao, T.; Whitehead, S.; Berg, A. C.; Lo, W.-Y.; Dollár, P.; and Girshick, R. 2023. Segment Anything. *arXiv:2304.02643*.
- Knapitsch, A.; Park, J.; Zhou, Q.-Y.; and Koltun, V. 2017. Tanks and Temples: Benchmarking Large-Scale Scene Reconstruction. *ACM Transactions on Graphics*, 36(4).
- Labe, I.; Issachar, N.; Lang, I.; and Benaim, S. 2024. DGD: Dynamic 3D Gaussians Distillation. *arXiv:2405.19321*.
- Li, Y.; and Pathak, D. 2024. Object-Aware Gaussian Splatting for Robotic Manipulation. In *ICRA 2024 Workshop on 3D Visual Representations for Robot Manipulation*.
- Li, Z.; Müller, T.; Evans, A.; Taylor, R. H.; Unberath, M.; Liu, M.-Y.; and Lin, C.-H. 2023. Neuralangelo: High-Fidelity Neural Surface Reconstruction. In *IEEE Conference on Computer Vision and Pattern Recognition (CVPR)*.
- Liu, K.; Zhan, F.; Zhang, J.; Xu, M.; Yu, Y.; Saddik, A. E.; Theobalt, C.; Xing, E.; and Lu, S. 2023. Weakly Supervised 3D Open-vocabulary Segmentation. *arXiv preprint arXiv:2305.14093*.
- Max, N. 1995. Optical models for direct volume rendering. *IEEE Transactions on Visualization and Computer Graphics*, 1(2): 99–108.
- Mildenhall, B.; Srinivasan, P. P.; Tancik, M.; Barron, J. T.; Ramamoorthi, R.; and Ng, R. 2020. NeRF: Representing Scenes as Neural Radiance Fields for View Synthesis. In *ECCV*.
- Müller, T.; Evans, A.; Schied, C.; and Keller, A. 2022. Instant Neural Graphics Primitives with a Multiresolution Hash Encoding. *ACM Trans. Graph.*, 41(4): 102:1–102:15.
- Niemeyer, M.; Manhardt, F.; Rakotosaona, M.-J.; Oechsle, M.; Duckworth, D.; Gosula, R.; Tateno, K.; Bates, J.; Kaeser, D.; and Tombari, F. 2024. RadSplat: Radiance Field-Informed Gaussian Splatting for Robust Real-Time Rendering with 900+ FPS. *arXiv.org*.
- Qin, M.; Li, W.; Zhou, J.; Wang, H.; and Pfister, H. 2023. LangSplat: 3D Language Gaussian Splatting. *arXiv preprint arXiv:2312.16084*.
- Qu, Y.; Dai, S.; Li, X.; Lin, J.; Cao, L.; Zhang, S.; and Ji, R. 2024. GOI: Find 3D Gaussians of Interest with an Optimizable Open-vocabulary Semantic-space Hyperplane. *arXiv:2405.17596*.
- Radford, A.; Kim, J. W.; Hallacy, C.; Ramesh, A.; Goh, G.; Agarwal, S.; Sastry, G.; Askell, A.; Mishkin, P.; Clark, J.; Krueger, G.; and Sutskever, I. 2021. Learning Transferable Visual Models From Natural Language Supervision. *arXiv:2103.00020*.
- Rashid, A.; Sharma, S.; Kim, C. M.; Kerr, J.; Chen, L. Y.; Kanazawa, A.; and Goldberg, K. 2023. Language Embedded Radiance Fields for Zero-Shot Task-Oriented Grasping. In *7th Annual Conference on Robot Learning*.
- Schönberger, J. L.; and Frahm, J.-M. 2016. Structure-from-Motion Revisited. In *Conference on Computer Vision and Pattern Recognition (CVPR)*.
- Shi, J.-C.; Wang, M.; Duan, H.-B.; and Guan, S.-H. 2023. Language Embedded 3D Gaussians for Open-Vocabulary Scene Understanding. *arXiv:2311.18482*.
- Takmaz, A.; Fedele, E.; Sumner, R. W.; Pollefeys, M.; Tombari, F.; and Engelmann, F. 2023. OpenMask3D: Open-Vocabulary 3D Instance Segmentation. *arXiv:2306.13631*.
- Tancik, M.; Weber, E.; Ng, E.; Li, R.; Yi, B.; Kerr, J.; Wang, T.; Kristoffersen, A.; Austin, J.; Salahi, K.; Ahuja, A.; McAllister, D.; and Kanazawa, A. 2023. Nerfstudio: A Modular Framework for Neural Radiance Field Development. In *ACM SIGGRAPH 2023 Conference Proceedings, SIGGRAPH '23*.
- van Oort, T.; Miller, D.; Browne, W. N.; Marticorena, N.; Haviland, J.; and Suenderhauf, N. 2024. Open-Vocabulary Part-Based Grasping. *arXiv:2406.05951*.
- Wang, Y.; Li, Z.; Zhang, M.; Driggs-Campbell, K.; Wu, J.; Fei-Fei, L.; and Li, Y. 2023. D³Fields: Dynamic 3D Descriptor Fields for Zero-Shot Generalizable Robotic Manipulation. *arXiv preprint arXiv:2309.16118*.

Ye, M.; Danelljan, M.; Yu, F.; and Ke, L. 2023. Gaussian Grouping: Segment and Edit Anything in 3D Scenes. *arXiv preprint arXiv:2312.00732*.

Ye, V.; and Kanazawa, A. 2023. Mathematical Supplement for the `gsplat` Library. *arXiv:2312.02121*.

Ye, V.; Li, R.; Kerr, J.; Turkulainen, M.; Yi, B.; Pan, Z.; Seiskari, O.; Ye, J.; Hu, J.; Tancik, M.; and Kanazawa, A. 2024. `gsplat`: An Open-Source Library for Gaussian Splatting. *arXiv:2409.06765*.

Zhang, H.; Li, F.; and Ahuja, N. 2024. Open-NeRF: Towards Open Vocabulary NeRF Decomposition. In *Proceedings of the IEEE/CVF Winter Conference on Applications of Computer Vision*, 3456–3465.

Zheng, Y.; Chen, X.; Zheng, Y.; Gu, S.; Yang, R.; Jin, B.; Li, P.; Zhong, C.; Wang, Z.; Liu, L.; Yang, C.; Wang, D.; Chen, Z.; Long, X.; and Wang, M. 2024. GaussianGrasper: 3D Language Gaussian Splatting for Open-vocabulary Robotic Grasping. *arXiv:2403.09637*.

Zhi, S.; Laidlow, T.; Leutenegger, S.; and Davison, A. J. 2021. In-place scene labelling and understanding with implicit scene representation. In *Proceedings of the IEEE/CVF International Conference on Computer Vision*, 15838–15847.

Zhou, S.; Chang, H.; Jiang, S.; Fan, Z.; Zhu, Z.; Xu, D.; Chari, P.; You, S.; Wang, Z.; and Kadambi, A. 2023. Feature 3DGS: Supercharging 3D Gaussian Splatting to Enable Distilled Feature Fields. *arXiv preprint arXiv:2312.03203*.

Zuo, X.; Samangouei, P.; Zhou, Y.; Di, Y.; and Li, M. 2024. FMGS: Foundation Model Embedded 3D Gaussian Splatting for Holistic 3D Scene Understanding. *arXiv:2401.01970*.

Method	Replica	LERF	3D-OVS
LERF	0.50	0.50	0.50
OpenNeRF	0.50	0.50	0.50
Ours- <i>NeRF</i>	0.55	0.60	0.55
LEGaussians	0.50	0.50	0.50
LangSplat	0.40	0.40	0.40
Ours- <i>3DGS</i>	0.60	0.60	0.55

Table 9: Selected Thresholds in Quantitative Results.

A Experiments Details

A.1 Implementation Details

We train the NeRF and the CLIP branch jointly from scratch with the same configurations of LERF except the learning rate on Replica datasets which is $1e-4$. The CLIP features are extracted using OpenCLIP ViT-B/16 trained on LAION-2B. We use an automatic mask generator from ViT-H SAM with the default configuration.

We optimize 3DGS in Section 3.4 with the same settings as the official 3DGS, except for the following modifications: 1) freezing the position of the Gaussian center \mathbf{x} , 2) setting the rotation learning rate to $1e-4$, and 3) running for 10K iterations without a densification process.

We train our models and competitors with a single RTX A5000.

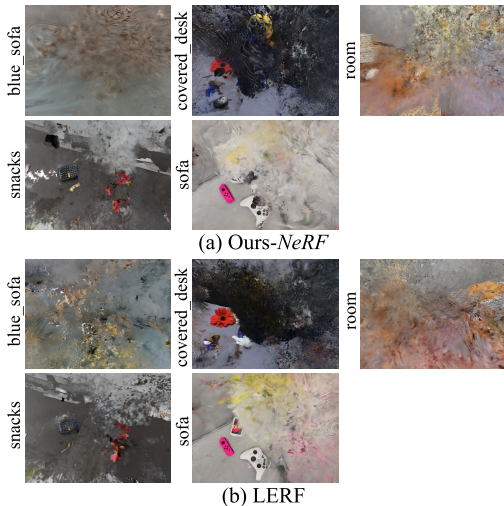


Figure 5: Poor reconstruction quality in evaluation view of 3D-OVS dataset.

A.2 Details of Datasets

We use three datasets for evaluation: Replica dataset for 3D segmentation, and LERF and 3D-OVS datasets for rendered 2D segmentation. All of these datasets are widely used to evaluate the segmentation performance of radiance fields. We fix the thresholds for each dataset as detailed in Table 9 to evaluate the performance.

Replica dataset. Replica dataset is a high-quality indoor 3D mesh dataset with semantic labels. We measure 3D segmentation performance with labeled 3D mesh, using class names as the text queries.

LERF dataset. LERF dataset is a collection of real-world scenes captured by iPhone. This includes text queries and their ground truth 2D bounding boxes. In LERF dataset, most competitors (Qin et al. 2023; Shi et al. 2023) report their performance by building their own ground truth mask datasets corresponding to their partly chosen text queries. However, it is a challenge to compare because the performance of open-vocabulary segmentation can significantly vary depending on the text query.

Hence, starting from the given text queries and 2D bounding boxes, we use SAM to create auxiliary masks and manually correct errors. SAM(Kirillov et al. 2023) receives an image and a user prompt (bounding box or point) as input and creates three masks. Among these candidate masks, we select the ground truth mask that corresponds most closely to the queried object. Then, we manually label a few inaccurate masks. The masks will be publicly available. We use four scenes *figurines*, *ramen*, *teatime*, *waldo_kitchen* from LERF dataset. We choose three evaluation views that are not blurry. These masks will be publicly available online.

3D-OVS dataset. 3D-OVS dataset is a collection of real-world scenes, text queries, and their ground truth pixel-level labels. The dataset consists of 10 scenes, each with 20-30 viewpoints, including five evaluation viewpoints. Several scenes in 3D-OVS dataset show poor reconstruction quality from the evaluation view shown in Figure 5. Therefore, we report the performance only for the scenes with successful reconstruction: (*bed*, *bench*, *lawn*, and *office_desk*).

ScanNet dataset. ScanNet dataset is a real-world dataset that includes RGB-D scans, meshes, and instance-level semantic labels. It is widely used to evaluate performance in 3D scene understanding tasks. In our case, we select one scene (*scene0003*) and provide the 3D segmentation accuracy, in Appendix C.

B Details of Previous Language Embed 3DGS

B.1 Splatting High Dimensions Embeddings on 3DGS

To jointly train 3DGS with language features, a straightforward approach is to embed the 512-dimensional language feature into each Gaussian. However, this approach results in out-of-memory(OOM) issues. Splatting 512-dimensional language embeddings requires 522 KB of shared memory per streaming multiprocessor (SM). Specifically, 3DGS (Kerbl et al. 2023) requires 10 KB of shared memory and needs an additional 1 KB/SM for each increase in the dimension of the language feature. 3DGS allocates static shared memory, and CUDA limits this allocation to 48 KB for architectural compatibility. Even with a dynamic allocation that enables allocation above the 48 KB limit, 522 KB of shared memory exceeds the maximum shared memory of

<i>figurines</i>	green apple, ice cream cone, jake, miffy, old camera, pikachu, pink ice cream, porcelain hand, quilted pumpkin, rabbit, red apple, rubber duck, rubics cube, spatula, tesla door handle, toy cat statue, toy chair, toy elephant, twizzlers, waldo
<i>ramen</i>	bowl, broth, chopsticks, egg, glass of water, green onion, napkin, nori, pork belly, ramen, sake cup, wavy noodles
<i>teatime</i>	bag of cookies, bear nose, coffee, coffee mug, cookies on a plate, dall-e, hooves, paper napkin, plate, sheep, spill, spoon handle, stuffed bear, tea in a glass, yellow pouf
<i>waldo_kitchen</i>	blue hydroflask, coffee grinder, cookbooks, cooking tongs, copper-bottom pot, dish soap, faucet, knives, olive oil, paper towel roll, pepper mill, pour-over vessel, power outlet, red mug, scrub brush, sink, spice rack, utensils, vegetable oil, waldo

Table 10: Text Query of LERF Dataset.

current top GPUs (e.g., the H100 has a maximum shared memory of 228 KB).

Consequently, existing methods address these challenges using the following strategies, each with its trade-offs:

- **Compress high-dimensional features** (Qin et al. 2023; Shi et al. 2023). This approach accelerates training but reduces segmentation performance and requires an additional decoding process.
- **Allocate rasterizer variables for the backward pass to global memory instead of shared memory** (Zhou et al. 2023). While this avoids performance degradation, it significantly slows down training.
- **Use dynamic shared memory allocation with reduced file size in the rasterizer** (Ye et al. 2024). This method is faster than global memory allocation while using more shared memory, but it still slows down training due to the smaller tile size.
- **Render in chunks** (Bhalgat et al. 2024). Although this accelerates training and prevents performance degradation, it drops fps (10 fps reported in the original paper).

Compressing the features produces poor mIoU (-7.30) but speeds up the training time $47\times$, as shown in Table 11. However, Ours-3DGS achieves fast training without feature compression.

Method	mIoU \uparrow	mAP \uparrow	Training Time \downarrow
3dim-feature	31.54	30.09	30 mins
512dim-feature	38.84	38.20	1400 mins

Table 11: Trade-off of Feature Compression on LERF dataset: we compress the feature following LangSplat while training each model with the same number of Gaussians for a fair comparison.

B.2 Post-process of LangSplat

We show the performance difference with and without post-processing in LangSplat, as shown in Figure 6. Without post-processing, it achieves a fast rendering speed of 55

fps ($550\times$)⁴ but produces a poor mIoU (-5.5) as shown in Table 12. Note that Ours-3DGS achieve faster rendering speed even compared to LangSplat without post-processing, as shown in Table 3.

LangSplat	mIoU \uparrow	mAP \uparrow
w/ post-process	37.53	36.39
w/o post-process	32.01	30.64

Table 12: Post-process of LangSplat on LERF dataset.

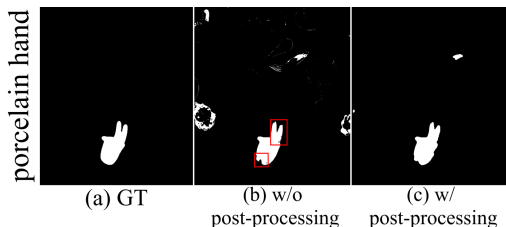


Figure 6: LangSplat includes post-processing, which significantly improves performance by reducing floaters.

C More Results

We mainly evaluate 3D segmentation accuracy on Replica datasets. To expand this, we also evaluate and compare on scene_0003 of ScanNet (Dai et al. 2017) dataset, in Table 13.

Additionally, we report the quantitative results of each scene on Replica dataset, LERF dataset, and 3D-OVS dataset, in Table 14-16.

⁴The post-processing consists of a mean convolution filter on the relevancy map implemented with OpenCV (61.98ms) and a mean convolution filter on the binary mask implemented with nested for-loops (3249 ms). This is done for three scales, 10473 ms in total.

Backbone	Method	ScanNet F1-score \uparrow
NeRF	LERF	0.0333
	OpenNeRF	0.0663
	Ours-NeRF	0.0849
3DGS	LEGaussians	0.0064
	LangSplat	0.0340
	Ours-3DGS	0.0769

Table 13: 3D Segmentation Accuracy Comparison on ScanNet dataset.

Backbone	Method	<i>office_0</i> F1-score \uparrow	<i>office_1</i> F1-score \uparrow	<i>office_2</i> F1-score \uparrow	<i>office_3</i> F1-score \uparrow
NeRF	LERF	0.0774	0.0191	0.0644	0.0621
	OpenNeRF	0.0486	0.0169	0.0318	0.0356
	Ours-NeRF	0.1434	0.0434	0.1493	0.1255
3DGS	LEGaussians	0.0013	0.0043	0.0109	0.0031
	LangSplat	0.0004	0.0123	0.0044	0.0038
	Ours-3DGS	<u>0.1097</u>	<u>0.0406</u>	<u>0.1395</u>	<u>0.1181</u>

Backbone	Method	<i>office_4</i> F1-score \uparrow	<i>room_0</i> F1-score \uparrow	<i>room_1</i> F1-score \uparrow	<i>room_2</i> F1-score \uparrow
NeRF	LERF	0.0645	0.1124	<u>0.1607</u>	0.1158
	OpenNeRF	0.0521	0.0180	0.0432	0.0423
	Ours-NeRF	0.1722	0.1654	0.1934	0.2232
3DGS	LEGaussians	0.0111	0.0080	0.0066	0.0085
	LangSplat	0.0107	0.0139	0.0122	0.0118
	Ours-3DGS	<u>0.1629</u>	<u>0.1636</u>	0.1529	<u>0.1959</u>

Table 14: Per-scene quantitative results on Replica dataset.

Method	<i>figurines</i>		<i>ramen</i>		<i>teatime</i>		<i>waldo_kitchen</i>	
	mIoU \uparrow	mAP \uparrow	mIoU \uparrow	mAP \uparrow	mIoU \uparrow	mAP \uparrow	mIoU \uparrow	mAP \uparrow
LERF	40.67	38.75	24.56	24.35	36.85	35.06	25.44	23.62
OpenNeRF	16.24	16.02	23.05	23.57	39.08	38.26	27.69	25.50
Ours-NeRF	59.79	59.00	37.44	38.38	47.59	46.92	<u>40.67</u>	<u>39.16</u>
LEGaussians	21.02	20.57	24.90	24.67	24.50	24.09	15.28	13.89
LangSplat	42.23	40.55	48.17	48.71	37.74	36.26	21.98	20.05
Ours-3DGS	<u>56.23</u>	<u>55.79</u>	<u>38.28</u>	<u>40.81</u>	<u>41.59</u>	<u>41.16</u>	42.60	41.79

Table 15: Per-scene quantitative results on LERF dataset.

Method	<i>bed</i>		<i>bench</i>		<i>lawn</i>		<i>office_desk</i>	
	mIoU \uparrow	mAP \uparrow	mIoU \uparrow	mAP \uparrow	mIoU \uparrow	mAP \uparrow	mIoU \uparrow	mAP \uparrow
LERF	45.29	57.74	50.88	51.59	54.19	57.40	60.04	61.41
OpenNeRF	82.25	82.40	<u>70.24</u>	71.14	78.70	79.27	69.29	69.79
Ours-NeRF	66.71	78.65	<u>66.69</u>	78.81	96.74	96.98	79.72	<u>84.18</u>
LEGaussians	33.23	44.94	63.86	64.25	43.48	44.20	51.36	50.05
LangSplat	65.74	73.01	82.75	88.06	82.41	87.95	67.26	68.93
Ours-3DGS	<u>67.40</u>	<u>79.33</u>	67.08	<u>79.20</u>	<u>96.25</u>	<u>96.92</u>	<u>78.89</u>	84.36

Table 16: Per-scene quantitative results on 3D-OVS dataset.